

Fiber Deflection Probe for Small Hole Metrology

B. Muralikrishnan^{1*}, J. A. Stone², J. R. Stoup²

¹Department of Mechanical Engineering & Engineering Science, UNC Charlotte, Charlotte NC 28223

²Precision Engineering Division, National Institute of Standards and Technology, Gaithersburg, MD 20899

Abstract

This paper presents the development of a new probing method for Coordinate Measuring Machines (CMM) to inspect the diameter and form of small holes. The technique, referred to as Fiber Deflection Probing (FDP), can be used for holes of approximately 100 μm nominal diameter. The expanded uncertainty obtained using this method is 0.07 μm ($k = 2$) on diameter. The probing system consists of a transversely illuminated fiber (with a ball mounted on the end) whose shadows are imaged using a camera. We can infer the deflection of the probe from the motion of the image seen by the camera, and we infer the position of the measured surface by adding the fiber deflection along x and y directions to the machine scale readings. The advantage of this technique is the large aspect ratio attainable (5mm deep for a 100 μm diameter hole). Also, by utilizing the fiber as a cylindrical lens, we obtain sharp crisp images of the fiber position, thus enabling high resolution for measured probe deflection. Another potential advantage of the probe is that it exerts an exceptionally low force (ranging from a few micronewtons down to hundreds of nanonewtons). Furthermore, the probe is relatively robust, capable of surviving more than 1 mm over-travel, and the probe should be inexpensive to replace if it is broken. In this paper, we describe the measurement principle and provide an analysis of the imaging process. Subsequently we discuss data obtained from characterization and validation experiments. Finally we demonstrate the utility of this technique for small hole metrology by measuring the internal geometry of a 129 μm diameter fiber ferrule and conclude with an uncertainty budget.

Keywords: Coordinate Metrology, Small Hole, Microfeature Metrology, Fiber Probe

1. Introduction

Measurement of diameter and form of small holes is of great importance in applications such as fuel injector nozzles, fiber optic ferrules, wire drawing dies, holes in printed circuit boards and medical apparatus such as syringes etc. Holes with large aspect ratios (depth/diameter) cannot readily be inspected by microscopes and require development of special sensors. The Moore M48 [1] Coordinate Measuring Machine (CMM) with a 0.3 mm diameter probe has been used at the National Institute of Standards and Technology (NIST). The relatively large contact forces in these probing systems and stiffness issues with thinner styli are primary limitations in measuring smaller features. While traditional probe-stylus combinations for the CMM cannot be used for smaller holes because of this limitation, the literature shows a variety of novel probes with thinner styli that have been constructed and mounted on a CMM. In such cases, the probe is mounted on the ram of

* Present address: Precision Engineering Division, National Institute of Standards and Technology, Gaithersburg MD 20899, email: balam@nist.gov

the machine with the part on the table or vice versa. The CMM is used as a fine positioning system with stylus deflection on contact detected by the new probe. Zhang and Yang [2] and later Yang *et al* [3] report a probe for the measurement of holes of diameter 200 μm with an accuracy of approximately 1 μm . The probe is modeled as an elastic body whose deflections are sensed using capacitance sensors. Masuzawa *et al* [4] report a vibroscanning method for measuring smaller holes. This technology uses a vibrating micro probe that contacts an electrically conducting surface. Upon contact, the circuit closes, thus sending out a signal. The signal is intermittent as the probe is vibrating. The duration of contact with the surface in relation to the time for one amplitude of probe vibration provides an index of proximity of the probe to the surface. Masuzawa *et al* [4] refined this technique using a twin probe to measure non-conducting surfaces as well. The vibroscanning technology is capable of measuring holes of approximately 125 μm diameter with an accuracy of 0.5 μm . In a related development, Lebrasseur *et al* [6] report on two other probing techniques. The first uses a piezoresistive cantilever as the probe while the other method uses stress induced shift in resonant frequency as the probing mechanism. In another novel development, Takaya *et al* [7] and Hashimoto *et al* [8] report on a probing technique based on optically trapping a small particle. In this technique, a particle trapped optically at a fiber tip is used as a probe. Theoretical formulation and preliminary analysis only have been reported in this area.

Physikalisch-Technische Bundesanstalt (PTB) has recently reported on the development of a fiber probing technique [9] with sub-micrometer uncertainties to measure holes of approximately 50 μm diameter. A thin fiber (15 μm diameter) with a ball (25 μm diameter) on the end is used as the probe. Light enters through the fiber and is incident on the ball. The back scattered light is imaged using a Charge Coupled Device (CCD) camera. The clear advantage of this technique is that the position of the ball is directly observed, thus requiring minimal contact forces and eliminating any sensitivity loss. Another recent development is the use of MEMs based technologies for dimensional measurement of micro features. Brand *et al* [10] developed a micro probe mounted on a thin wafer whose deflections are detected by piezoresistors embedded in the wafer. Haitjema *et al* [11, 12] report on the development of new probes that use strain gages embedded in tiny flexures that support the probe. These probes have nanometer resolutions and a claimed uncertainty on the order of 0.1 μm (probe nonlinearity is on the order of 10 nm).

There is also literature on small hole measurement capabilities by National Measurement Institutes (NMI) around the world. In a recent international comparison conducted by PTB [13], six European national metrology institutes measured ring gages between 0.1 mm and 1 mm diameter. The expanded uncertainty ($k = 2$) on the smallest hole (100 μm nominal diameter) is between 1 μm and 3.8 μm .

Many of the techniques reported in the literature address the challenge of measuring small holes with large aspect ratios but have large uncertainties. MEMS based probes with strain gages are expected to have superior performance as demonstrated by [11, 12], but are expensive to manufacture. In this paper, a new probing method is proposed that addresses both the aspect ratio and uncertainty issue in small hole metrology. We refer to

this method as Fiber Deflection Probing (FDP). The technique differs from the method described in [9] (developed at PTB) in that we monitor the position of the fiber stem, a few millimeters from the ball, in two orthogonal directions, instead of observing the ball directly. By illuminating the probe stem in a plane perpendicular to the fiber, we are able to travel deep into the hole (a depth of approximately 5 mm into a 100 μm hole), without being limited by diffraction effects in the case of back-scattered light from the ball. Also, by utilizing the fiber stem as a cylindrical lens, we are able to obtain a sharp image of the fiber's position to enhance edge detection. Our technique is simple, inexpensive to develop and yields an expanded uncertainty of 0.07 μm ($k = 2$) for holes of diameter 100 μm .

Some of the basic ideas behind inferring the fiber probe position by observing the fiber stem have been described previously in [14,15] and also in a patent held by Werth Messtechnik GmbH [16]. The use of the stem as a cylindrical lens to focus light for clear edge determination was first described in [17]. In subsequent sections, we discuss the principle of this technique, construction details, characterization and validation results. Finally, we demonstrate the utility of this technique by discussing measurement results from a 129 μm fiber ferrule hole and conclude with an uncertainty budget.

2. Fiber Deflection Measurement

2.1 Principle

A thin glass fiber, cantilevered at one end and with a ball mounted on the other, serves as the probe. A small segment of this fiber is illuminated by a laser diode as shown in Fig. 1 a short distance below the ball. The shadow of the fiber is magnified and imaged using a camera. When the probe contacts a surface, it is deflected by a small amount. The magnitude of this deflection is determined by recording the position of the fiber in the free state and in the deflected state. This deflection is then corrected from final machine coordinates to obtain the position of the surface.

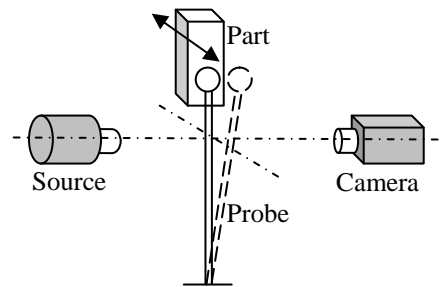


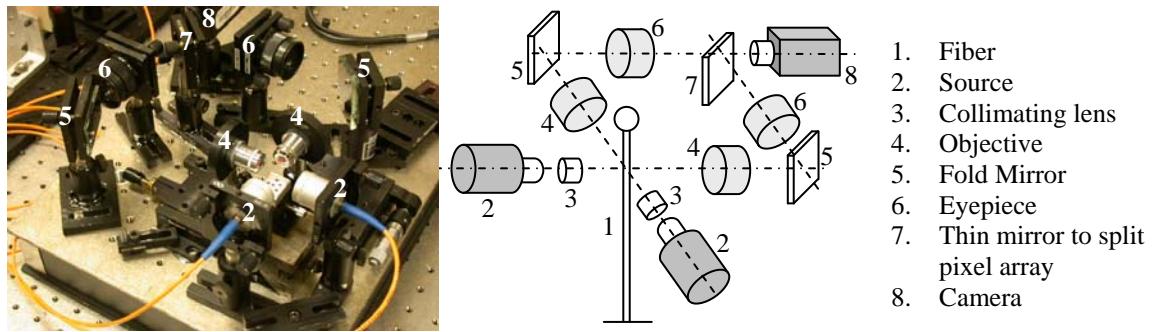
Fig. 1 Measurement principle

2.2 Optical Setup

The optical setup is illustrated in Fig. 2. Collimated beams from two orthogonal directions illuminate the fiber approximately 5 mm below the ball. The shadows of the stem are magnified using 7X objectives (4) placed in front of the fiber. The resulting

images are further magnified using 5X eyepieces (6) and imaged using a CCD camera. The mirror (7) in front of the camera (8) extends half way across the pixel array, so that light from one axis illuminates half of the array and light from the second axis falls on the other half of the array.

The use of one camera for imaging the fiber from both directions places a constraint on the amount of magnification achievable. Each half of the pixel array should not only be able to image the full width of the stem in its null position, but also when the probe deflects by approximately $25\ \mu\text{m}$ in each direction. Monitoring the outer boundaries of the shadow is not feasible under this constraint. We instead determine the fiber position using a thin band of light visible on the center of the fiber shadow in the image plane. The formation of this band is discussed in the next section.



(a) (b)
Fig. 2 Optical setup for fiber deflection measurement (a) Photo and (b) Schematic

2.3 Imaging Analysis

Fig. 3 shows typical distances of the lenses and image plane, along with a screen shot of the fiber stem's shadow at the image plane. From geometrical optics, the stem undergoes a magnification of 35 and this is also verified experimentally. Also seen in Fig. 3 is a thin band of light in the middle of the shadow of the stem. This band is produced by refraction of the source at the leading edge of the glass fiber and again at the trailing edge, as shown in Fig. 3. For purposes of this analysis, it is assumed that a collimated beam is incident on the fiber. Consider a ray at a distance X from the optical axis. The normal at the point of contact with the fiber makes an angle α_1 as shown in Fig. 3. Then, from the law of refraction,

$$\beta_1 = \sin^{-1}(\sin(\alpha_1)/\mu) \quad (1)$$

where μ is the refractive index of glass. The refracted beam strikes the fiber again at the right edge and undergoes a second refraction. Because triangle OAB is an isosceles triangle and from the law of refraction,

$$\beta_2 = \sin^{-1}(\mu \sin(\beta_1)) \quad (2)$$

$$\alpha_2 = 2\beta_1 - \alpha_1 \quad (3)$$

The refracted ray finally makes an angle ϕ with the axis, where ϕ is given by

$$\phi = \beta_2 - \alpha_2 \quad (4)$$

The position where the ray strikes the axis, measured from the fiber center, is computed using Eq. 5 below:

$$Y = \frac{R \sin(\alpha_2)}{\tan(\beta_2 - \alpha_2)} + R \cos(\alpha_2) \quad (5)$$

From Eq. 5, an incident ray close to the axis (say, $X = 10 \mu\text{m}$) meets the axis farther away after double refraction and at smaller angles than another ray farther away (say, $X = 20 \mu\text{m}$). As a consequence of this aberration (which is the two-dimensional analog of the aberrations of a small ball lens in three dimensions), the light emerging from the $50 \mu\text{m}$ fiber is focused to a minimum size on the order of $8 \mu\text{m}$ width and then diverges. However, if we restrict our attention to rays that can enter our 0.2 N.A. objective lens, then ray tracing shows that the minimum line width is reduced from $8 \mu\text{m}$ to 90 nm . In the geometric optics limit, the width of the image on our camera can then be found by multiplying the 90 nm line width following the fiber by the lateral magnification of the microscope. (Note: we have verified through ray tracing that multiplying by the magnification gives the correct answer for our microscope.) This predicts a width of $3.1 \mu\text{m}$ for the bright line on the pixel array.

The actual smallest width of the bright band on the CCD array, as observed experimentally, is approximately $125 \mu\text{m}$. While ray tracing indicates that it should be possible to tune the objective position to obtain a width of $3.1 \mu\text{m}$ at the image plane, diffraction effects dominate in our system. The diameter of the Airy disk for N.A.= 0.2 and red light illumination is about $3.6 \mu\text{m}$. This value is much larger than 90 nm , which is the smallest width of the band we are trying to image. Therefore, diffraction will dominate over the effects of aberrations for our system with N.A.=0.2. At a magnification of 35, diffraction should limit the width of the image to about $125 \mu\text{m}$, equivalent to 15 pixels, which is roughly what we see experimentally. The diffraction limit is here much larger than the pixel size, suggesting that we might be able to reduce the magnification without degrading performance. However, we have thus far not been successful in doing this.

When we image only the bright band at the center of the fiber, the diffraction from the edges of the fiber is not important because it does not overlap the image of the central bright band. If we image the entire fiber, diffraction patterns are indeed seen along the edges, and this might limit our ability to define the position of the fiber if we were to use the outside edge of the full fiber for measurement. However, our only requirement is to reproducibly observe *changes* in the fiber position, which are not affected by a constant diffraction pattern. Furthermore, we are somewhat immune to details of the imaging of the fiber edges if we determine the position of the center line of the fiber by averaging the positions of the two edges, so that any diffraction-induced shift in the apparent position of one edge is cancelled by a similar shift of the position of the opposite edge. More importantly, averaging two edges provides some immunity to variations in illumination and in defocus. (This is true whether we are using the entire fiber or the central bright band.)

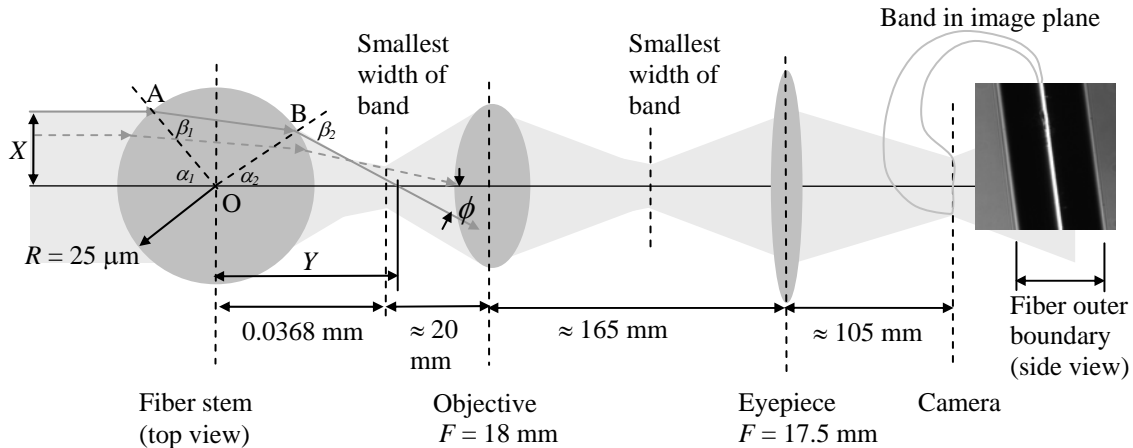


Figure 3. Typical distances of lenses and camera from fiber center (diagram not to scale) as seen in top view. A ray striking the fiber at a distance X meets the optical axis at a distance Y and at an angle ϕ after double refraction. A ray closer to the axis meets the axis at a point farther from the fiber center. Thus, the light entering the objective is not a point source. This aberration produces a thin band of light in the middle of the stem's shadow at any image plane. For a $50 \mu\text{m}$ diameter fiber, the smallest width of the band occurs at 0.0368 mm from the fiber center. The objective focuses on this band to produce an intermediate image, which is then magnified by the eyepiece.

2.4 Image Processing

The shadows of the fiber stem, as projected onto the camera, appear as a dark region with a bright band down the center. When working in two dimensions, two bands are seen on the camera, as shown in Fig. 4 (a). Our normal method of conditioning the image involves three steps. (1) We determine a threshold value related to the intensity distribution of the image. (2) Based on this threshold, we convert the image from 8-bit gray scale to a binary bright/dark image. (3) We then apply a particle-removal function to suppress the influence of any dirt particles. The resulting image is shown in Fig. 4 (b). The second step, converting the image from a graduated gray scale to bright/dark, seems to be helpful for successful particle removal in the third step. There is some danger that the second step will degrade performance due to loss of subpixel information, but the loss is minimal if the fiber is angled slightly so that the image does not align exactly with a column of pixels. We have found that analysis of subpixel information can improve performance under special circumstances but is not helpful for our normal measurements.

After conditioning the image, the leading and trailing edge coordinates for both bright bands are determined for each horizontal pixel row. This information is used (through least squares fitting and averaging) to determine the center pixel of each of the bands at the center row. The center pixel coordinates so obtained, are monitored before and after fiber deflection to obtain the magnitude of CMM over travel.

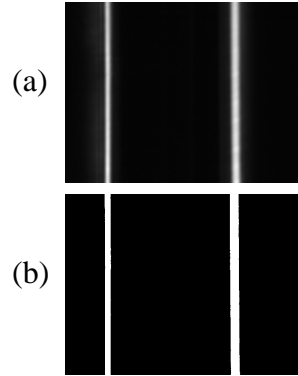


Figure 4 (a) Image as recorded by the camera (b) Binary image after processing

2.5 Imaging Uncertainty

While an uncertainty budget for diameter and radial out-of-roundness (OOR) measurements is presented later on, we discuss the uncertainty in determining the fiber center due to imaging to understand the performance of the system. The system has an optical magnification of approximately 35. The width of each pixel in the camera is 8500 nm. Thus, single-pixel resolution is $8500/35 \approx 243$ nm when sub-pixel interpolation is not employed. Therefore, the center can lie within -122 nm and $+122$ nm with equal probability. Assuming a rectangular distribution, the standard uncertainty is $122/\sqrt{3} \approx 70$ nm. This is the uncertainty in determining the center using just one row of pixels. We average over 400 rows to reduce this uncertainty. In the absence of noise, the reduction in uncertainty due to averaging is a complex function of the angle of the fiber relative to the pixel array. If the fiber is tilted relative to the pixel array so that it crosses more than three pixels in the horizontal direction, then the error due to pixel resolution is reduced below ± 0.04 pixels (± 10 nm). Assuming a rectangular distribution of errors, this ± 10 nm range of possible errors corresponds to a standard uncertainty of 6 nm. For some angles the uncertainty might be considerably smaller, but as long as the angle is large enough that at least three horizontal pixels are crossed, the uncertainty will not exceed this value. Also, as a consequence of the fact that we measure both the left and right edge of the band, the uncertainty will be reduced to a value on the order of $(6/\sqrt{2})$ nm ≈ 4 nm. Thus we might hope to see roughly a 4 nm uncertainty in detecting the position of the probe in space under ideal conditions. We have carried out measurements that indicate that this small uncertainty for the imaging system is probably attainable, but under realistic conditions our uncertainties are much larger due to other factors, with the imaging uncertainty contributing negligibly to the overall uncertainty budget. Although the 4 nm uncertainty might be improved further by sophisticated sub-pixel interpolation, there is no practical advantage to doing so.

3. Fiber Probe

3.1 Probe Manufacture

The early experiments used a 30 mm long, 125 μm diameter glass fiber with a 155 μm diameter ball on the end. The later experiments used a 20 mm long, 50 μm diameter glass fiber with a 75 μm diameter ball on the end. Early versions of the probe are manufactured by melting a ball at the end of the fiber using a blowtorch. This method does not adequately center the ball on the fiber. The second version with thin glass fibers (50 μm diameter, 20 mm long) is made in-house by gluing a microsphere to the end of a fiber.

The method developed here uses the existing optical setup to also manufacture the probes but with one small modification. Because it is necessary to image the entire ball and the fiber stem from two directions, the eyepieces are removed to reduce the magnification. The microsphere is placed on a small flat shiny surface and its images along two perpendicular directions are obtained on the monitor. The fiber is brought down from the top using a 3-axis stage. The fiber is dipped in epoxy, with the excess glue removed prior to bonding with the microsphere. Fig. 5 shows images of a fiber before and after bonding to a microsphere. In each of the figures, (a) and (b), two orthogonal views of the same fiber-microsphere are shown.

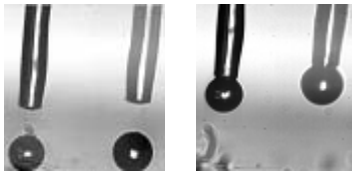


Fig. 5 Orthogonal views of the fiber and microsphere (a) Before bonding (b) After bonding (Stem ϕ 50 μm and ball ϕ 75 μm)

3.2 Probe contact force and resonant frequency

The contact force for a 125 μm diameter, 30 mm long fiber stem made of glass ($E = 80$ GPa) assuming typical deflections of 20 μm is 2 μN . For a 20 mm long, 50 μm diameter stem, the contact force is only 0.2 μN . When the probe is not in contact with a surface, the resonant frequency for a 125 μm diameter probe with a 155 μm ball is 695 Hz (4366 rad/sec) while it is 625 Hz (3928 rad/sec) for a 50 μm probe with a 75 μm ball on the end. A high resonant frequency is desirable, although we have not seen degradation in performance at lower resonant frequencies. The extremely small contact forces prevent part damage during measurement of microstructures and also eliminate the need for any deformation corrections. The very low effective mass of the fiber probes (on the order of 24 μg) is also important, as this reduces inertial impact forces when the probe hits a surface.

4. 1D Characterization of the system

Before the system is mounted on a CMM for rigorous testing, 1D performance is evaluated using a piezo stage (Fig. 6). An arm is mounted on the piezo stage and is aligned parallel to one optical axis of the deflection system. A retro reflector is held at the end of this arm and a 5 mm steel ball is glued to the backside of the retro reflector. The ball serves the function of a test surface and is centered on the retro reflector to essentially measure at zero Abbe offset. The ball is brought in contact with the fiber, which is deflected by moving the piezo stage. The actual distance traveled by the stage is monitored using a laser interferometer. This setup is used for calibration (determining a scale factor that relates displacement of probe stem in pixels to displacement of the tip in micrometers) in one axis (active axis) and also to subsequently evaluate linearity in that axis.

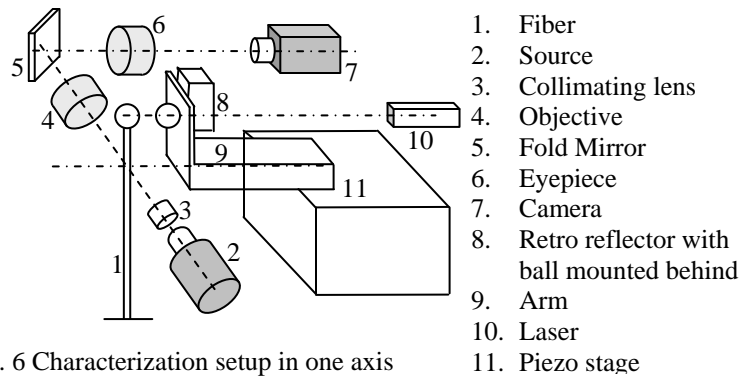


Fig. 6 Characterization setup in one axis

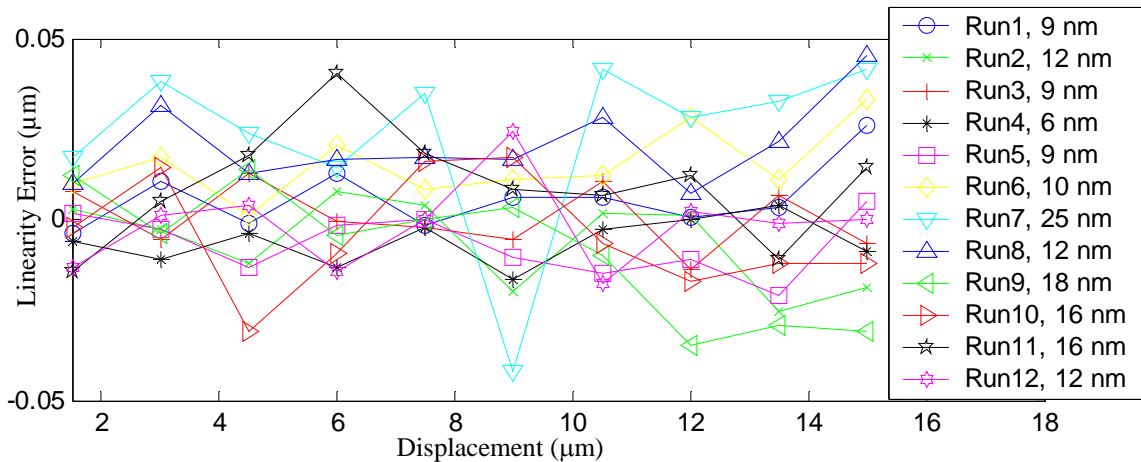


Fig. 7. Long-term linearity results in 1D (legend shows standard deviation for each run). The scale factor was determined earlier to be $0.2750 \mu\text{m}/\text{pixel}$.

Fig. 7 shows 12 runs where the apparent position of a surface is measured as a function of probe displacement. The data was acquired over a 40 min period. The data gives some indication as to the magnitude of the errors that can be expected to occur after calibration of the probe, including errors that might arise from random noise, nonlinearity, hysteresis, or variations in the calibration factor.

Each of the 12 runs consists of 11 data points taken at displacements ranging up to 15 μm . At each point, the probe reading, multiplied by the scale factor, is added to the interferometer reading to give the apparent position of the surface in contact with the probe. In the absence of errors, this value would be a constant independent of probe displacement. In the graph, we have subtracted a constant so that the reading should be zero for all points, and the deviations shown in the graph are thus the errors due to nonlinearity or non-repeatability of the data. We use the same probe calibration factor for all the runs. We have subtracted a different constant for each run so as to eliminate the effect of a drift in our test apparatus. (The test apparatus had much greater drift than was observed in actual measurements on the machine.)

For each run, we compute the standard deviation of the data points, and this is shown in Fig. 7. It is seen that one standard deviation is between 6 nm and 25 nm for each run in this test. From Fig. 7, it is seen that there are no clear systematic effects in the linearity plot. The deviations shown in the diagram do not repeat well from one run to the next, indicating that the deviations arise primarily from random noise. For the entire data set comprising all 12 runs, one standard deviation is 17 nm.

5. 2D Characterization of the system

After the system is mounted on the CMM, scale factors are first determined using a procedure similar to that described earlier. However, the CMM is used as the positioning stage instead of the piezo. Also, unlike in the 1D case where only one scale factor was determined, scale factors are determined in both axes. In fact, because the optical magnifications are not identical for both axes and the point of observation on the fiber is also slightly different, scale factors are expected to be slightly different for each axis. In order to obtain a more robust estimate, scale factors are determined in four principal directions (+x, -x, +y, -y) and pairs are averaged to obtain estimates for x and y .

After obtaining the scale factors, a quick experiment to determine repeatability is conducted. The CMM is moved along positive x to the same coordinate several times, bringing the probe repeatedly into contact with a surface. The standard uncertainty due to repeatability is approximately 35 nm. This includes the machine positioning repeatability term (≈ 25 nm) and any surface effects such as slip because the probe loses contact with the part before each run.

In order to assess the performance of the system in 2D, linearity tests are conducted on the CMM. A 3 mm ruby sphere is used as the test artifact for this study. The ball is brought in contact with the probe from positive x direction and the probe is deflected approximately 21 μm . On the return path, 5 linearity data points are collected at a spacing of 3 μm . This procedure is repeated for each of the other three principal directions and the cycle is repeated 5 times. The deviation from linearity along each direction is shown in Fig. 8. It is seen that one standard deviation out-of-linearity error is of the order of 20 nm to 50 nm. This is slightly larger than the results obtained from 1D tests; the marginally better performance in the piezo test bed is probably due to better

environmental control around the probe as the entire assembly can be shielded from air currents, a situation not feasible on the CMM. Also, a portion of the linearity error on the CMM can be attributed to the machine’s positioning repeatability (≈ 25 nm) itself.

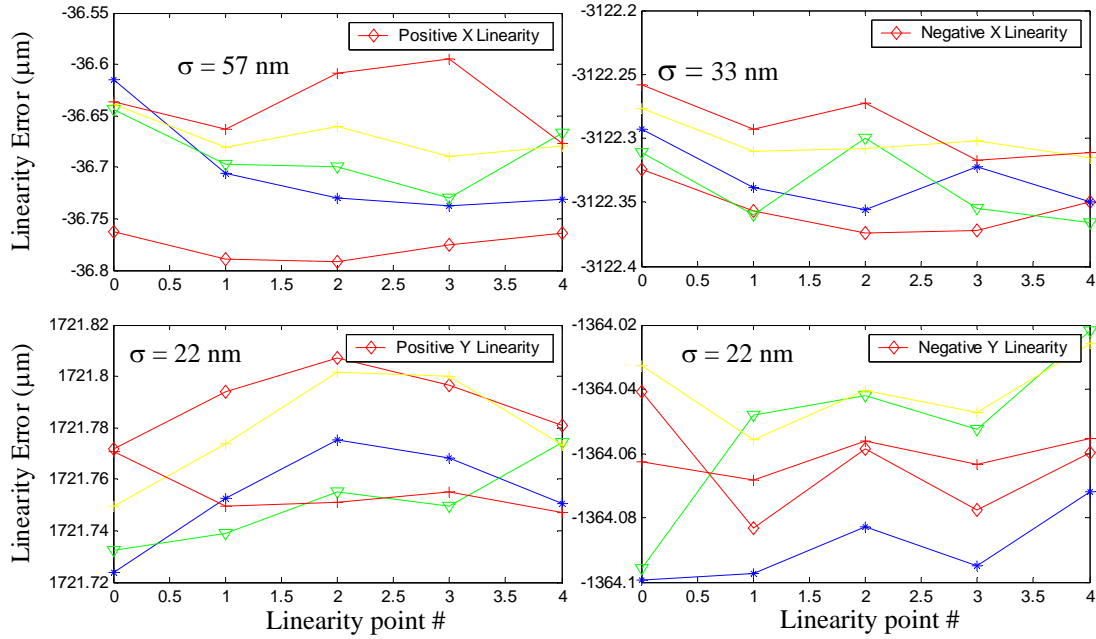


Figure 8. Linearity testing results in 2D

6. Validation Measurements

In order to validate the probing system, three artifacts of known diameter and form are measured using the FDP. Prior to each of these measurements, the fiber probe tip diameter and the form of the probe tip are calibrated by using a 3 mm ruby sphere of known diameter and form. The diameter of the calibration ball is measured using interferometry at NIST with an expanded uncertainty of $0.01 \mu\text{m}$ ($k = 2$). Table 1 shows a comparison of diameters obtained using FDP and other techniques. The agreement in diameters is to within 60 nm, which is smaller than the uncertainty of the measurements itself.

Table 1 Comparison of diameters obtained using FDP and other sources

Artifact	Dia from other sources (μm)	Dia from FDP (μm)	Difference (μm)
5 mm Sphere 1	4999.98 (UMM ¹) ± 0.09	4999.92 ± 0.07	0.06 ± 0.15
1 mm Hole	999.53 (M48 CMM ²) ± 0.15	999.48 ± 0.07	0.05 ± 0.17
5 mm Sphere 2	5000.19 (UMM ¹) ± 0.09	5000.15 ± 0.07	0.04 ± 0.15

¹UMM – Universal Measuring Machine at NIST. Two point diameters are measured at 10 locations and averaged. ²Moore M48 CMM at NIST is used to measure the hole. The number following the symbol \pm is the expanded uncertainty ($k = 2$).

Fig. 9, 10 and 11 provide more information on each of these measurements. They show the form error of the fiber ball estimated during calibration, the residual form on the test artifact and diameter information.

The '5 mm sphere 1' and '1 mm hole' artifacts are measured using a larger fiber probe. The fiber probe ball diameter is calibrated before measuring each test artifact. The values obtained are $155.12 \pm 0.05 \mu\text{m}$ and $155.09 \pm 0.05 \mu\text{m}$, well within the uncertainty of the measurement. The form errors on the fiber ball are shown in Fig 9 (a) and 10 (a). The third artifact '5 mm sphere 2' is measured using a smaller fiber probe and its form error is noticeably different, as seen in Fig. 11 (a). Also, each of the measurements reported here, both calibration and test artifact measurement, is the average of many runs. Typical one standard deviation repeatability in diameter is of the order of 10 nm to 20 nm over 3 to 5 runs and these are also recorded in the figures.

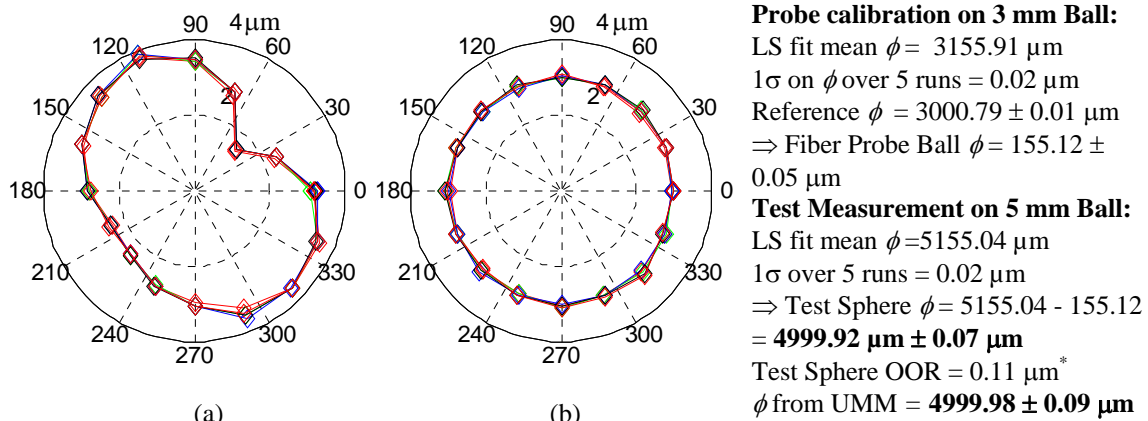


Figure 9 Measurements on '5 mm sphere 1' artifact (a) Probe ball form error (b) Form error on 5mm ball [The number following \pm is the expanded uncertainty ($k = 2$)], * OOR uncertainty not evaluated yet

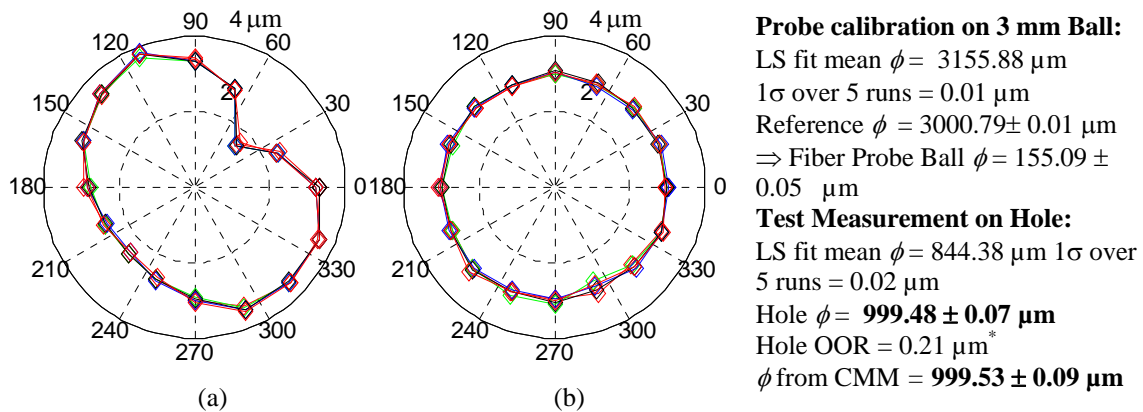
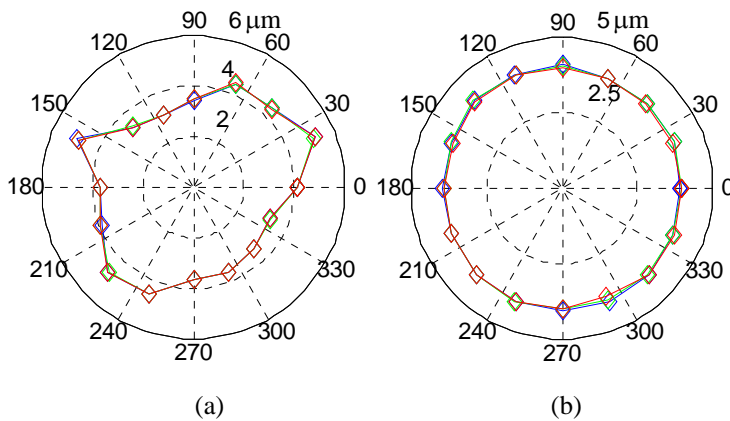


Figure 10 Measurements on '1mm hole' artifact (a) Probe ball form error (b) Form error on hole [The number following \pm is the expanded uncertainty ($k = 2$)], * OOR uncertainty not evaluated yet



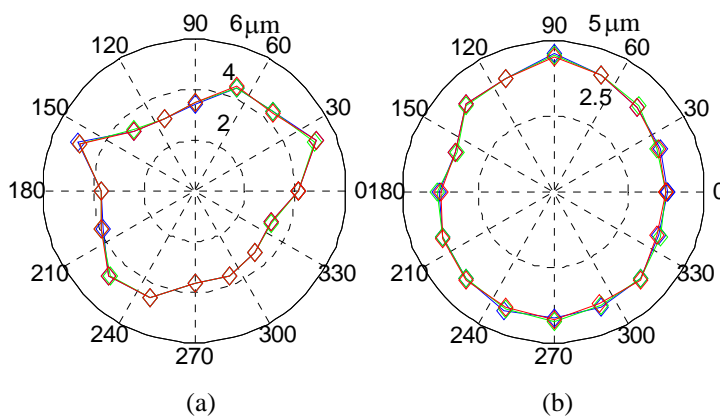
Probe calibration on 3 mm Ball:
 LS fit mean $\phi = 3088.12 \mu\text{m}$
 1σ on ϕ over 3 runs = $0.01 \mu\text{m}$
 Reference $\phi = 3000.79 \pm 0.01 \mu\text{m}$
 \Rightarrow Fiber Probe Ball $\phi = 87.33 \pm 0.05 \mu\text{m}$
Test Measurement on 5 mm Ball:
 LS fit mean $\phi = 5087.48$
 1σ over 3 runs = $0.02 \mu\text{m}$
 Test Sphere $\phi = 5000.15 \pm 0.07 \mu\text{m}$
 Test Sphere OOR = $0.18 \mu\text{m}^*$
 ϕ from UMM = $5000.19 \pm 0.09 \mu\text{m}$

Figure 11 Measurements on ‘5 mm sphere 2’ artifact (a) Probe ball form error (b) Form error on 5mm ball [The number following \pm is the expanded uncertainty ($k = 2$)], * OOR uncertainty not evaluated yet

7. Small hole measurement

After validating the probing system using the different artifacts, we demonstrate the utility of the probe for small hole metrology by measuring the internal geometry of a ceramic fiber ferrule with a nominal diameter of $129 \mu\text{m}$. We discuss preliminary measurements and potential issues here.

The fiber ferrule hole is located by simply centering the fiber using the outer surface of the ferrule. Because the inner surface is concentric with the outer surface to within $2 \mu\text{m}$, location of the hole is relatively simple and does not require any special optics. The fiber is inserted $80 \mu\text{m}$ inside the hole and a measurement is made. The diameter obtained is $129.58 \mu\text{m}$ and the form error is $1.04 \mu\text{m}$ (radial OOR). This is shown in Fig. 12. These values are not yet verified using other techniques.



Probe calibration on 3 mm Ball:
 LS fit mean $\phi = 3088.12 \mu\text{m}$
 1σ on ϕ over 3 runs = $0.01 \mu\text{m}$
 Reference $\phi = 3000.79 \pm 0.01 \mu\text{m}$
 \Rightarrow Fiber Probe Ball $\phi = 87.33 \pm 0.05 \mu\text{m}$
Test Measurement on ferrule:
 LS fit mean $\phi = 42.25 \mu\text{m}$
 1σ over 3 runs = $0.01 \mu\text{m}$
 Test Hole $\phi = 42.25 + 87.33 =$
 $129.58 \pm 0.07 \mu\text{m}$
 Test Hole OOR = $1.04 \mu\text{m}^*$

Figure 12 (a) Probe form error (b) Form error on $129 \mu\text{m}$ fiber ferrule hole [The number following \pm is the expanded uncertainty ($k = 2$)], * OOR uncertainty not evaluated yet

The FDP is subsequently used to measure the inside geometry of a different ferrule by measuring traces at multiple heights as shown in Fig. 13. The visible tilt in the axis is

attributed to the misalignment of the hole with the machine's axis. We have not created a reference datum for this measurement and therefore rely on aligning the probe and the hole with the machine's axis. While misalignment of the hole's axis will manifest itself as tilt in the measured data, any misalignment in the probe's stem will result in the probe shanking at larger depths. There is evidence of this effect in Fig. 13 with profiles at larger depths showing two outlier points, an effect not as evident in the profile near the mouth of the hole (trace corresponding to $Z = 30 \mu\text{m}$). And finally, the data also indicates a piece of dirt at a depth of $130 \mu\text{m}$ as shown in Fig. 13. Dirt appears to be a potential problem with periodic cleaning of the part and the fiber ball necessary to obtain outlier free data. The diameter values reported in Fig. 13 are computed on 14 sampling points, omitting the 2 points that indicate stem shanking.

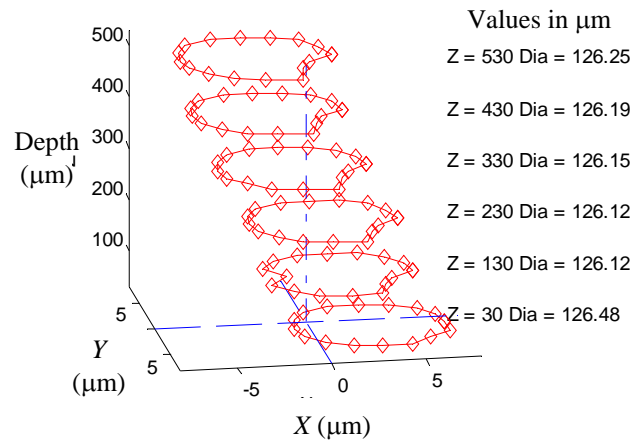


Fig. 13 Measured ferrule geometry over 0.5 mm depth. Profile at $Z = 30 \mu\text{m}$ is near the mouth of the hole. [uncertainty in diameter for each trace is $0.07 \mu\text{m}$, $k=2$]

8. Uncertainty Analysis

In this section, we outline an uncertainty budget for diameter measurement using the FDP. For this discussion, we consider measurements on a $100 \mu\text{m}$ ceramic ferrule. A 20 mm long, $50 \mu\text{m}$ diameter glass fiber with an $80 \mu\text{m}$ ball on the end is considered as the probe. Probe ball diameter and radial form error calibration are performed using a 3 mm ruby sphere. Table 2 lists sources that contribute to uncertainty in diameter of the test artifact. From Table 2, the combined standard uncertainty is 34 nm on diameter of test artifact. Thus, the expanded uncertainty is $0.07 \mu\text{m}$ ($k = 2$) on diameter. We present a short overview of the sources of error here; more detailed discussion can be found in [16].

A large contributor to the uncertainty in diameter is single point repeatability (experimentally determined to be approximately 35 nm); this is primarily due to the machine position repeatability (25 nm) and imaging uncertainty (4 nm). Thus, the uncertainty in determining every coordinate in space is approximately 35 nm. From Monte Carlo simulation (MCS) using Gaussian noise, this translates to 18 nm standard uncertainty in best-fit diameter (using 16 sampling points). This term is counted twice, once for the calibration artifact and again for the test artifact.

There is an error associated with determining the scale factor (in units of $\mu\text{m}/\text{pixel}$). This error will not influence diameter if the same scale factor value is used during calibration and subsequent test artifact measurement. This is true under the circumstance that the fiber deflects by the same nominal amount at all angular positions (sampling locations) of both the master ball and test artifact. In reality, the fiber will not deflect by identical amounts at all angular positions of any artifact because of centering and part form error. The contribution of this term is therefore listed in the table.

The contribution to diameter uncertainty from master ball diameter error is approximately 5 nm. The error in determining the master ball's equatorial plane is assumed to be about $\pm 1.5 \mu\text{m}$, which results in a standard uncertainty of about 1 nm in diameter. Similarly, the tilt in the test hole's axis is assumed to be $\pm 0.5^\circ$, resulting in 1 nm standard uncertainty in diameter. Temperature effects are typically not significant for dimensional measurement of small objects. Assuming $\pm 0.05^\circ\text{C}$ fluctuations in temperature, the standard uncertainty in determining master ball diameter because of non-standard temperature is 1 nm.

The optical axes of the probe measurement system will not necessarily be perpendicular to each other. Also, the axes will not be aligned with the machine's axes. The offset angles can be estimated by analyzing the data obtained from the 4 principal machine directions. We typically software correct axis misalignment based on such experimental data. Assuming an uncertainty of $\pm 0.5^\circ$ in determining the offset angles, the net effect is 1 nm standard uncertainty in diameter. If the test artifact and the calibration sphere are of approximately the same size, this effect is almost canceled out.

Experimentally, we have determined the standard uncertainty in diameter to be of the order of 20 nm. This repeatability samples the different error sources we have outlined in previous sections. It is however possible that there are other sources we have not sampled. To account for these, we itemize a 20 nm uncertainty in diameter in our budget.

9. Conclusions

This paper presents the development of a novel probing method for CMMs to measure the diameter and form of small holes. The technique is based on imaging of a thin glass fiber stem. Holes of approximately 100 μm diameter can be measured to depths of about 5 mm using this method. Measurements are made on three artifacts, and diameters obtained using FDP agree with other techniques to within 60 nm. Using the probe, we have measured the diameter and inner geometry of a 125 μm nominal diameter fiber optic ferrule. Uncertainty budgets have been developed and they indicate an expanded uncertainty of 0.07 μm ($k = 2$) on diameter for 100 μm nominal diameter holes. We are currently studying the extension of this technique for profile and 3D measurement.

Acknowledgements: We are grateful to Dr. Wolfgang Haller, Jefferey Anderson and Eric Stanfield at NIST for valuable suggestions on manufacturing the fiber probe, drawing the glass fibers, and for reference diameter measurements respectively. We also thank Drs. Theodore Doiron, Steven Phillips and Johannes Soons at NIST for carefully reviewing the manuscript.

Table 2 Error sources contributing to uncertainty in diameter

	Error source	Description	Uncertainty (nm)
1	$u_{cal}(Coordinates)$	Uncertainty in probe ball diameter due to uncertainty in determining coordinates (X, Y) of probing points. This is primarily because of imaging uncertainty and machine repeatability.	18
2	$u(Coordinates)$	Same as 1, but on test artifact	18
2	$u(SF)$	Uncertainty in scale factor combined with centering error	1
		Uncertainty in scale factor combined with unequal nominal deflections between calibration and master ball	7
2	$u_{cal}(Height)$	Error in determining the equatorial plane (Z height) on master ball	1
3	$u_{cal}(Master)$	Uncertainty in master ball diameter and form	5
4	$u_{cal}(T)$	Uncertainty in diameter due to nonstandard temperature. This affects calibration sphere diameter primarily because of larger nominal diameter. Test artifact diameter is much smaller and temperature effects are ignored.	1
6	$u(Tilt)$	Error in determining tilt angle on test artifact	1
7	$u(AM)$	Probe axis misalignment introduces an error in diameter, some of which cancels out when measuring the cal-ball and later the test artifact. Also, most of this error is software corrected. The residual error is tabulated here.	1
8	$u(Other\ sources)$	Contribution from machine positioning and other sources	20

Subscript *cal* indicates calibration process

References

1. Commercial equipment and materials are identified in order to adequately specify certain procedures. In no case does such identification imply recommendation or endorsement by the National Institute of Standards and Technology, nor does it imply that the materials or equipment identified are necessarily the best available for the purpose.
2. G.X Zhang and S. M. Yang, A 3D Probe for Measuring Small Blind Holes, Annals of the CIRP, 44/1/1995, 461-464
3. S Yang, S Li, M J. Kaiser and E.H.K Fung, A probe for the measurement of diameters and form errors of small holes, Measurement Science and Technology, 9 (1998), 1365-1368
4. T Masuzawa, Y Hamasaki and M Fujino, Vibroscanning method for nondestructive measurement of small holes, Annals of the CIRP, 42/1/1993, 589-592
5. T. Masuzawa, B. J. Kim, C. Bergaud, M. Fujino, Twin-probe vibroscanning method for dimensional measurement of microholes, Annals of the CIRP 46/1/1997 437-440
6. E Lebrasseur, J-B Pourciel, T Bourouina, T Masuzawa and H Fujita, A new characterization tool for vertical profile measurement of high aspect ratio microstructures, J. Micromech. Microeng. 12 (2002) 280-285
7. Y Takaya, S Takahashi, T Miyoshi, K Saito, Development of the Nano-CMM probe based on laser trapping technology, Annals of the CIRP, 48/1/1999 421-424
8. T Hashimoto, Y Takaya, T Miyoshi, R Nakajima, Fundamental analysis on the novel 3-D probing technique for micro-parts using the optical fiber trapping, Proceedings of the annual meeting of the ASPE, 2003, 83-86

9. H. Schwenke, F. Waldele, C. Weiskirch, H. Kunzmann, Opto-tactile Sensor for 2D and 3D Measurement of Small Structures on Coordinate Measuring Machines, *Annals of the CIRP* 50/1/ 2001, 361-364
10. U Brand, T Kleine-Besten, H Schwenke, Development of a special CMM for Dimensional Metrology on microsystem components, *Proceedings of the Annual Meeting of the ASPE* 2000, 542-546
11. H Haitjema, W.O Pril, P.H.J. Schellekens, A Silicon-Etched Probe for 3-D Coordinate measurements with an Uncertainty Below 0.1 μm , *IEEE Transactions on Instrumentation and Measurement* 50 (6) December 2001, 1519-1523
12. H. Haitjema, W.O. Pril and P.H.J. Schellekens, Development of a Silicon-based Nanoprobe System for 3-D Measurements, *Annals of the CIRP* 50/1/2001, 365-368
13. M. Neugebauer and F. Ludicke, EUROMET comparison: diameter of small ring gauges, *Metrologia*, 2001, 38, 259-267
14. J A. Stone and S Vemuri, Stem bending contact probe, PTO Provisional Patent Serial Number 60/350,391, January 2002.
15. J A. Stone and S Vemuri, Ultra-low force probing for CMMs: studies of MEMS-based and fiber-bending probe systems, presentation at Measurement Science Conference, Anaheim, CA, January 2002
16. R Christoph, E Trapet, H Schwenke, US patent # 6651351, Coordinate measuring instrument with feeler element and optic sensor for measuring the position of the feeler.
17. B. Muralikrishnan, J. Stone, S. Vemuri, C. Sahay, A. Potluri, J. Stoup, Fiber deflection probe for small hole measurements, *Proceedings of the ASPE Annual Meeting*, 2004, 24-27
18. B. Muralikrishnan and J. Stone, Fiber Deflection Probe Uncertainty Analysis for Micro Holes, *Proceedings of the 2005 NCSL Workshop and Symposium*, Washington DC, August 7-11, 2005